Article

A Novel Shear Strengthening of Existing RC Shear Walls Using Steel Wire Mesh and Polymer Mortar

Xinyao Xie, Zixiong Guo *, Syed Humayun Basha [ID] and Qunxian Huang

College of Civil Engineering, Huaqiao University, Xiamen 361021, China; xxyao19@stu.hqu.edu.cn (X.X.);
syedhbasha@hqu.edu.cn (S.H.B.); huangqx@hqu.edu.cn (Q.H.)
* Correspondence: guozxcy@hqu.edu.cn

Abstract: A new type of strengthening technique for existing reinforced concrete (RC) shear walls was proposed using steel wire mesh (SWM) and polymer mortar. The experimental campaign consists of testing one conventional RC shear wall specimen and four specimens strengthened using different configurations of steel wire mesh ratios and wrapping methods under cyclic lateral loading. The experimental results showed that the application of steel wire meshes and polymer mortar not only delayed the shear cracks formation but also effectively controlled the crack propagation. The average increase in cracking load of strengthened specimens was about 79%. The lateral load-carrying capacity of the strengthened specimens increased (about 55%) with the increase in the considered steel wire mesh reinforcement ratio compared to the control specimen. Wrapping of steel wire meshes around the shear wall surface prevented debonding of polymer mortar layers, and enhanced the performance compared to wrapping only on exposed surfaces. A theoretical expression to estimate the capacity of the strengthened shear walls was proposed based on the softened strut-and-tie model. The proposed expression fairly predicted the capacity of the strengthened specimens for the present and previous study.

Keywords: RC shear walls; shear strengthening; steel wire mesh (SWM); strut-and-tie model (STM); shear capacity; polymer mortar

1. Introduction

Over the past several decades, comprehensive research studies on the seismic performance of RC shear wall structures have been conducted, and the advancements (e.g., extending the length of reinforcement along the cross-section of boundary elements and increasing the transverse reinforcement ratio to ensure sufficient deformation under high axial load ratios) cumulatively reflected in the current seismic design standards (ACI 318-19 [1], Eurocode 8 [2] and GB 50011-2010 [3]). Despite these improvements, there is still a huge stock of RC shear walls constructed following the less stringent previous national design standards. Recent earthquakes (Wenchuan 2008 [4], Chile 2010 [5], and New Zealand 2011 [6]) highlighted that existing RC shear wall structures were susceptible to severe damage or collapse due to insufficient shear reinforcement, deficient boundary elements, and no additional confinement at the ends [7]. Among the various deficiencies, brittle shear behavior due to insufficient transverse reinforcement ratio is a serious concern that may lead to high socio-economic consequences. Therefore, strengthening of vulnerable existing RC shear walls is of utmost importance to prevent brittle shear failure of structures in future earthquakes.

Extensive research has been conducted in the past decade to improve the seismic performance of RC shear walls in terms of shear strength, ductility, and energy dissipation [8–16]. Marini et al. [8] strengthened the existing RC shear walls using high-strength concrete jackets and numerically verified the strengthening option. It was reported that the strengthening method significantly improved the ultimate load-carrying capacity, deformation capacity, and ductility of strengthened shear walls. Altin et al. [9] and Christidis

et al. [10] utilized epoxy adhesives to fix steel strips on the surface of RC shear walls and observed that different steel strip configurations enhanced the lateral load behavior of the shear deficient RC wall. Recently, fiber reinforced polymer (FRP) has gained importance in strengthening of structural elements. To this date, a large number of studies have been carried out to evaluate the effectiveness and feasibility of FRP strengthening [11–16]. However, the major limitation of externally bonded strengthening methods is that they are susceptible to debonding, particularly under severe environments, and extensive application of adhesives impacted environmental protection.

The steel wire mesh (SWM) strengthening method has gained attention in recent years due to its advantages in terms of fire prevention [17] and favorable mechanical characteristics [18] compared to other externally bonding techniques. Few research studies have been dedicated to evaluate the effectiveness of the external steel wire mesh strengthening method in case of RC columns [19], beams [20,21], and masonry walls [22,23]. Most of these studies [19–23] demonstrated that SWM improved not only the load-carrying capacity but also the deformation capacity of the specimens to a particular extent. However, the application of the SWM strengthening method to improve the seismic behavior of shear deficient RC shear walls is not available. Henceforth, taking into account the advantages and further popularizing the application of this method, the authors adopted SWM to strengthen the existing RC shear wall structures. Further, polymer mortar has wide utilization prospects in seismic retrofitting and rehabilitation because of crack resistance, durability, and simple construction process [24,25]. Application of hanging SWM on the wall surface followed by smearing of polymer mortar over the surface was found to be the conventional strengthening methods [26,27], but such a technique may lead to the separation of strengthening layers under lateral loads. Therefore, to increase the utilization rate of materials and enhance the interface performance between the wall and strengthening layers, a novel reliable strengthening method was proposed by applying a moderate prestressing force so that the SWM remains in a tension state. Further, the steel wire mesh can be either wrapped around the surface of the wall along the height or applied on the exposed surfaces only based on the functional requirements, as shown in Figure 1a. When the ends of the RC shear wall are inaccessible (e.g., flanged and L-shaped shear wall), which make it cumbersome to apply SWM around the wall, strengthening only on exposed surfaces can be adopted (Figure 1b).
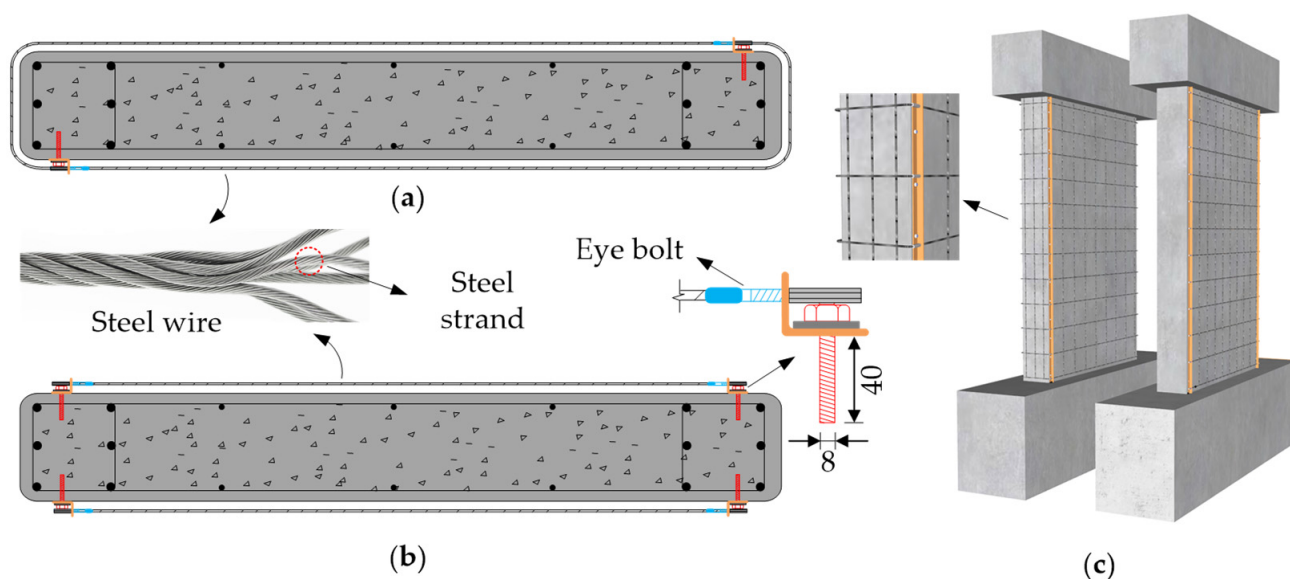

Figure 1. Adopted steel wire mesh strengthening method: (**a**) wrapping around surface; (**b**) wrapping only on exposed surfaces; (**c**) elevation.

The research reported in the present article aims to: evaluate the effectiveness and feasibility of steel wire mesh and polymer mortar by testing one control and four strengthened

RC shear wall specimens considering various configurations under cyclic lateral loads; study the failure progression, hysteretic and envelop lateral load-drift response, energy dissipation capacity and strain gauge recordings; analyze the influence of different parameters (steel wire mesh reinforcement ratio and wrapping method) on the behavior of shear walls; and propose an expression to predict the shear strength of the strengthened specimens.

2. Experimental Program

A total of five specimens, namely, one control specimen (SW1) and four strengthened specimens (SW2–SW5), were designed and tested in this experimental campaign. To simulate the deficiencies (e.g., insufficient shear reinforcement and low strength concrete) of existing shear walls, the specimens were designed based on the recommendations of less stringent previous national Chinese design standard JGJ 3-91 [28]. According to this code, the minimum value of concrete strength and thickness of shear wall were C20 and 160 mm, respectively. Considering the shear strengthening as the research objective of this test and the constraints of the laboratory and facilities, the shear span (height to width) ratio and section length of the specimens were selected as 1.62 and 1.00 m, respectively. Further, JGJ 3-91 [28] recommends the maximum spacing and the minimum diameter of horizontal and vertical reinforcement as 300 mm and 8 mm, respectively. Therefore, considering the reinforcement ratio limits, the horizontal- and vertical- reinforcement ratios were designed as 0.31% and 0.18%, respectively, to study the effectiveness and feasibility of the shear strengthening technique. Figure 2 shows the reinforcement details and the dimensions of the specimens. The aspect ratio (height to width) and the slenderness ratio (height to thickness) of the specimens was about 1.62 and 9.19, respectively.
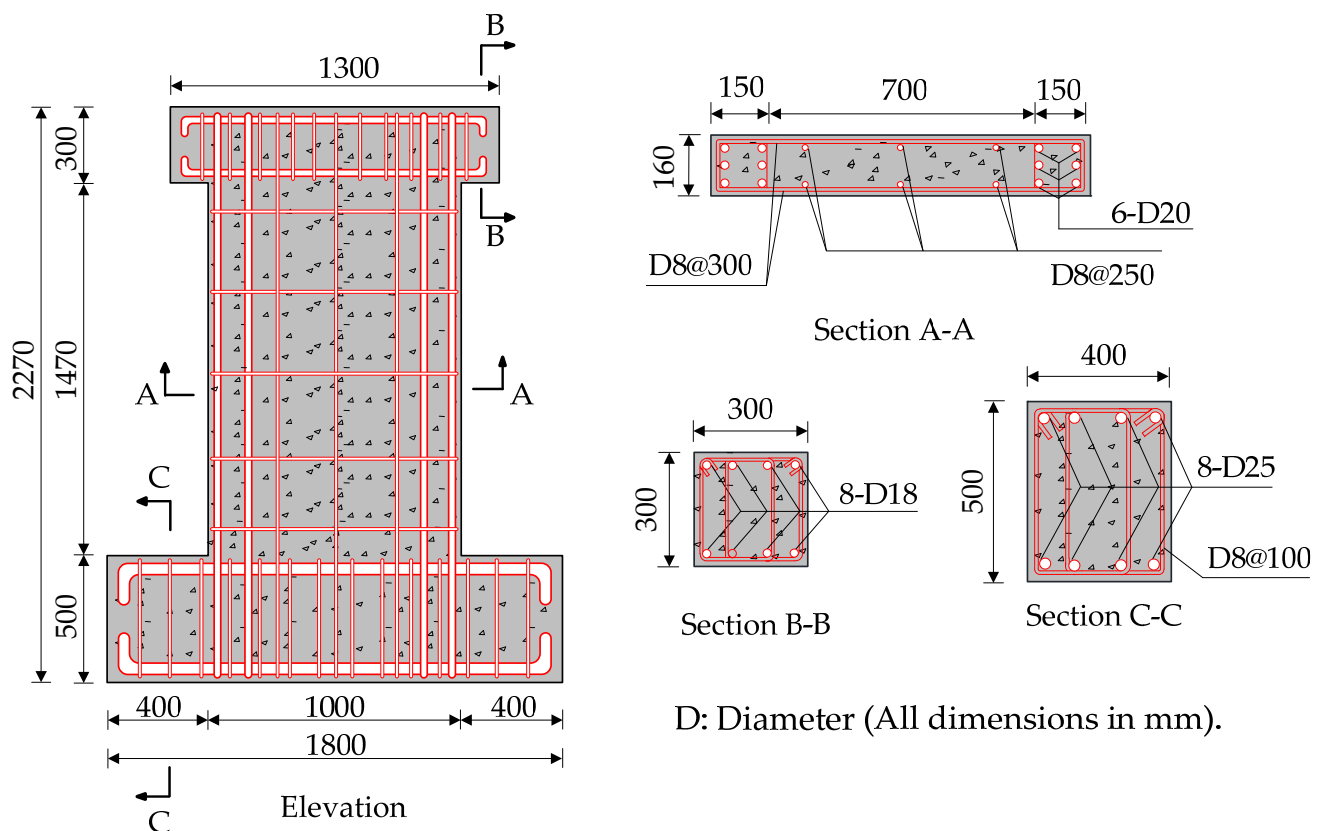

Figure 2. Reinforcement detailing of shear wall.

The test variables considered in the present study include the steel wire ratio and its application on the surfaces are given in Table 1. Two types of steel wire mesh application methods were adopted in the present study, i.e., wrapping around the surface of the

specimen using two anchor bolt systems and wrapping only on the exposed surfaces using four anchor bolt systems.

Table 1. Test variables of specimens.

Specimen Designation	Horizontal Steel Wire Configuration		Application of Steel Wire Mesh
	Diameter and Spacing (mm)	Steel Wire Mesh Ratio ρ_{swm} (%)	
SW-1	-	-	-
SW-2	4.0 @100	0.09	Wrapping around surface
SW-3	4.5 @60	0.20	Wrapping around surface
SW-4	4.5 @40	0.30	Wrapping around surface
SW-5	4.5 @40	0.30	Only on exposed surfaces

Note: ρ_{swm} is the ratio of steel wire mesh and is calculated as $\rho_{swm} = A_s/(b \times s)$, where A_s, b, and s are the cross-sectional area, thickness of the shear wall, and spacing between the steel wires, respectively.

To quickly and effectively realize the two wrapping methods, the specific construction procedure was carried out in five stages. In the first stage, the corners of the specimens were chamfered to reduce the stress concentration phenomenon and the bolt hole locations required to fix the anchoring systems were determined. In the second stage, holes were drilled in the wall along the height near the corners and the wall surfaces were gouged to increase the interface adhesion (Figure 3a). The wall surfaces and the bolt holes were cleaned to remove any loose material and dust. In the third stage, anchor bolts of 8 mm diameter were fixed into the holes, which were then further strengthened by using a strong commercially available marble glue. Later on, depending on the strengthening application, either two or four steel angles of size $30 \times 20 \times 3$ mm were bolted to the shear wall as soon as the strength requirements were met (Figure 3b).
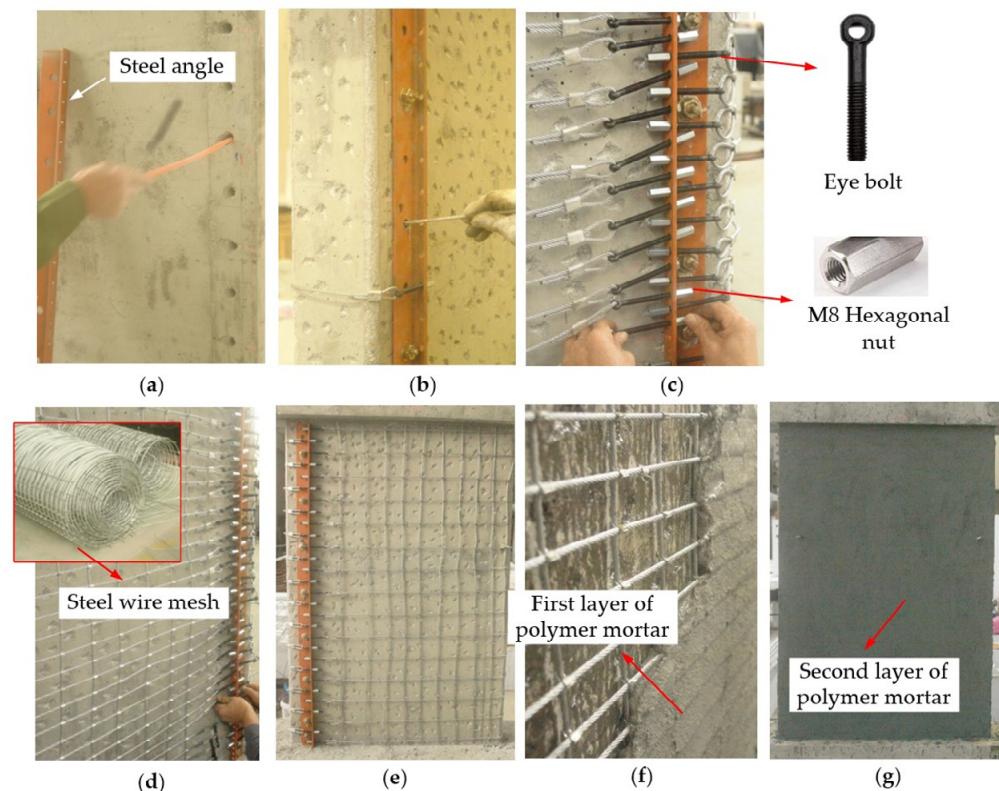

Figure 3. Strengthening process adopted: (**a**) drilling and cleaning of holes; (**b**) gouging the wall surface and fastening steel angles; (**c**) fastening the aluminum buckles; (**d**) wrapping of steel wire mesh; (**e**) tightened steel wire meshes; (**f**,**g**) first and second layer plastering of polymer mortar.

In the fourth stage, horizontal steel wires of the previously weaved mesh (Figure 3c) of required size and spacing (Table 1) were connected to an eye bolt using aluminum fasteners. Later on, the eye bolts were properly placed in the steel angles (Figure 3c) and were fastened with M8 hexagonal nuts using a torque wrench (Figure 3d). The same torque (about 1 kNm) was used to tighten all the steel wire meshes. In the fifth stage, cement slurry was sprayed over the wall surface followed by smearing of polymer mortar in two layers. The first layer of 15 mm thick polymer mortar was applied to cover the steel wire meshes and steel angles (Figure 3f). Environmental protection and smooth surface were ensured by plastering the second layer of 15 mm thick polymer mortar (Figure 3g).

In the present study, three types of steel wire mesh ratios (ρ_{swm}) were adopted in specimens SW2 (0.09%), SW3 (0.2%), SW4 (0.3%), and SW5 (0.3%) to evaluate the influence of the diameter (4 and 4.5 mm) and the spacing (100 mm, 60 mm, and 40 mm) of the steel wires. The details of the material characteristics of the shear wall specimens are given in Table 2. To comply with the low-strength characteristics and seismic deficient buildings, the specimens were constructed using normal-grade concrete.

Table 2. Summary of material characteristics.

Material Properties	Number of Specimens	Average Value	COV (%)
Compression strength of concrete (MPa)	9	19.6	5.6
Compressive strength of polymer mortar (MPa)	11	52.0	10.5
Elastic modulus of concrete (MPa)	3	2.55×10^4	12.3
Elastic modulus of polymer mortar (MPa)	3	3.3×10^4	16.1
Yield strength of 8 mm diameter steel bars (MPa)	3	441.0	2.4
Yield strength of 20 mm diameter steel bars (MPa)	3	448.3	0.6
Yield strain of 8 mm diameter steel bars ($\mu\varepsilon$)	3	2210.0	7.4
Yield strain of 20 mm diameter steel bars ($\mu\varepsilon$)	3	2240.0	3.1
Ultimate tensile strength of steel wire (MPa)	6	1100.0	6.1

The average 28 days compressive strength of 150 mm concrete cubes tested following GB/T 50,081 [29] was 19.6 MPa (COV 5.6%). Two-component polymer mortar was used in the present study and was obtained by mixing 1:6 ratio of emulsion and powder. The average compressive strength of polymer mortar cubes tested following JGJ/T 70 [30] was 52 MPa (COV 10.5%). The modulus of elasticity of concrete and polymer mortar from compressive tests were found to be 2.55×10^4 MPa (COV 12.3%) and 3.3×10^4 MPa (COV 16.1%), respectively. The properties of steel reinforcement obtained from tensile tests are given in Table 2. The ultimate tensile strength of the steel wire was found to be 1100 MPa (COV 6.1%).

Test Setup and Instrumentation

The schematic representation of the test setup is shown in Figure 4. The specimens were tested in slow-cyclic lateral loading under constant vertical compression at a loading speed of 0.15 mm/s. The lateral load was applied using a 1000 kN capacity MTS servo-controlled hydraulic actuator connected to the top concrete stub beam using six stiffened steel rods and two steel plates. The vertical compressive load was applied by a hydraulic jack attached to a frictionless sliding cart onto a spreader beam to distribute the compressive load uniformly (Figure 4a). The axial compression ratio *n* (calculated as the ratio of axial force to the cross-sectional area multiplied by the compressive strength of concrete) of all specimens was calculated as 0.1 and maintained constant throughout the test. The loading protocol adopted in the present study was in accordance with guidelines suggested in JGJ 101-96 [31]. A pre-compressive loading (0.33 of predetermined vertical load) was applied prior to the commencement of the test to check the pure axial compression state of the shear wall. Initially, the specimens were tested under force control mode consisting of one cycle for three different force levels of 50 kN, 100 kN, and 150 kN (Figure 5). Later on, the shear

walls were tested under displacement-control mode consisting of three cycles for each drift level (0.2%, 0.33%, 0.67%, 1%, 1.33%, and 2%).
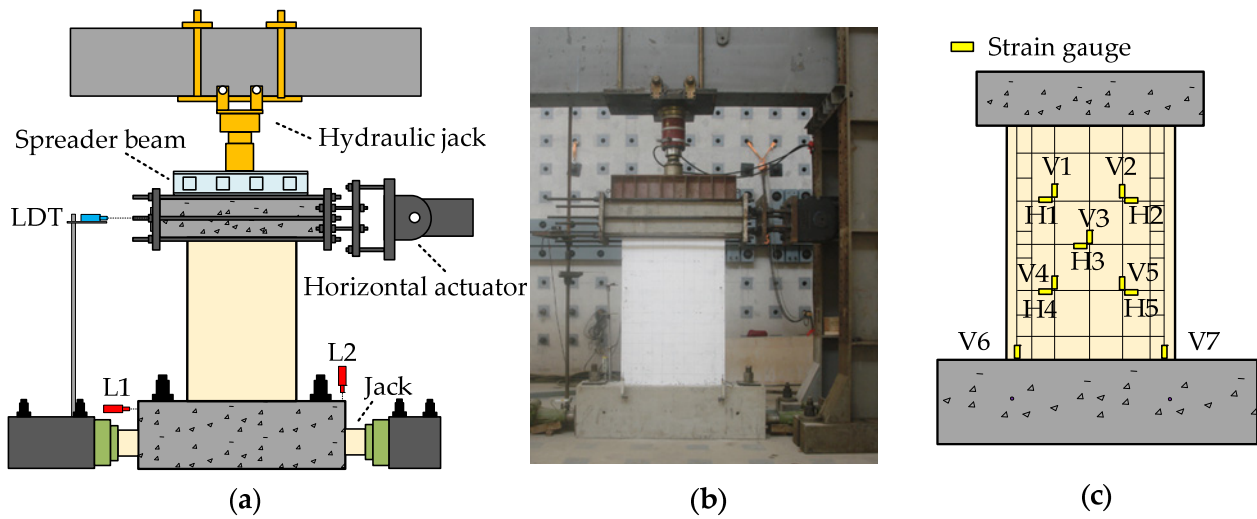

Figure 4. Test set-up: (**a**) schematic representation; (**b**) photograph of test setup; (**c**) layout of strain gauges.
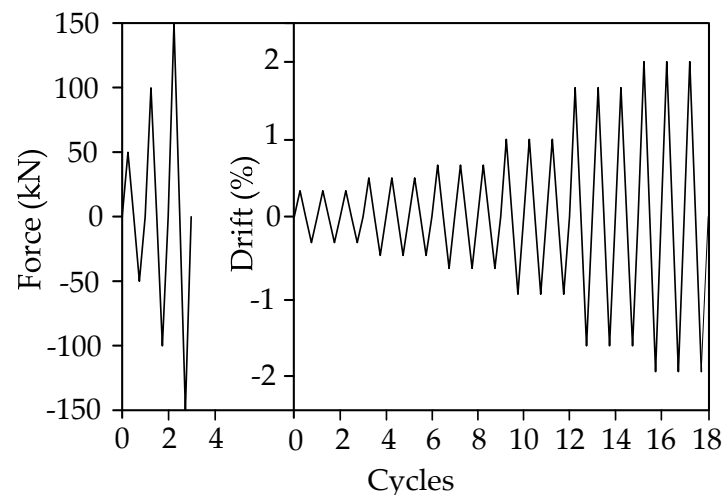

Figure 5. Adopted loading protocol.

The specimens were instrumented with linear variable displacement transducers (LVDTs), laser displacement transducer (LDT), strain gauges to monitor deformations and nonlinear behavior of the specimens. A LDT mounted near the mid-height of the top beam was used to calculate the drift of the specimens. LVDTs (L1 and L2) placed near the bottom beam were used to monitor the slip and warpage during the loading process (Figure 4). Strain gauges (V1 to V5, H1 to H5, and V6 to V7) were installed to monitor the development of the tensile strain in the specimens (Figure 4).

3. Experimental Observations

The experimental behavior of the strengthened shear wall specimens was discussed based on the initiation of major cracking followed by its propagation and subsequent failure mechanisms. As shown in Figure 6, the formation of cracks and its propagation in control and strengthened specimens were found to be different. In the control specimen SW1, cracks were initiated as flexural cracks along the height of the specimen corresponding to a lateral load of 150 kN in the force control mode. Whereas in strengthened specimens,

cracks were initiated in drift-controlled loading. In specimen SW2, flexural cracks were initiated at 0.2% drift (lateral load of 187 kN) slightly below the mid-height. Minor diagonal shear cracks were developed in specimen SW1 at 0.18% (178 kN) drift, whereas, in strengthened specimen SW2 shear cracks formed in the wall web at 0.27% (195 kN) drift. Multiple diagonal shear cracks were formed near the middle height of specimen SW1 corresponding to 0.33% (216 kN) drift. Subsequently, in specimen SW1, two major diagonal web-shear cracks in both the loading directions were formed at 1% (322 kN) drift and horizontal reinforcement started yielding (2212 μɛ). Spalling and crushing of concrete were observed near the left bottom of the shear wall at a drift level of 2% (342 kN) and the test was terminated at the same drift level. In specimen SW2 multiple diagonal shear cracks developed at 1.33% (380 kN) drift, which were absent in control specimen SW1. Finally, two major diagonal web-shear cracks were formed at 2% drift (468 kN). The intense cracking on the surface of strengthened specimen SW2 was mainly due to the presence of steel wire meshes acting as horizontal reinforcement and restraining the development of major diagonal web-shear cracks. No debonding between polymer mortar layers and concrete surface was observed in specimen SW2.
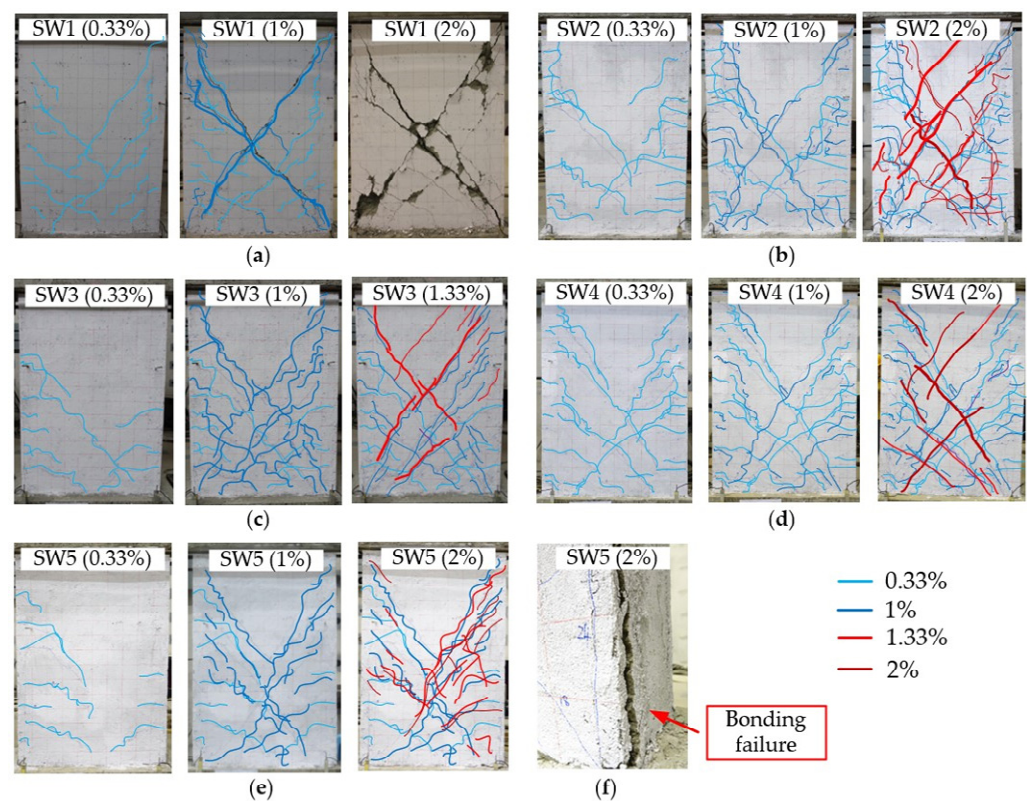

Figure 6. Crack patterns and failure mechanisms of specimens: (**a**) SW1; (**b**) SW2; (**c**) SW3; (**d**) SW4; (**e**) SW5; (**f**) debonding of polymer mortar layers in SW5.

In the case of higher SWM strengthening ratio specimens (SW3 and SW4), cracks were mainly originated either near the wall web or slightly below the mid-height of the shear wall. Flexural cracks formed initially near the mid-height of the shear wall at a drift of 0.25%. With increasing lateral drift (≥1%), flexural cracks propagated towards the opposite corners as flexure-shear cracks. Specimens (SW3 and SW4) observed flexure-shear cracks at 0.48% (311 kN) and 0.65% (342 kN) drift, respectively. Four major diagonal web-shear cracks were formed at 2% drift (541 kN) in specimen SW4. It was ascertained that the number of cracks in the shear wall web depends on the strengthening ratio of SWM. Minor flexure-shear cracks formed in the wall web in case of specimens SW3 and SW4 was found to be higher compared to specimen SW2. Most of the cracking was concentrated in the lower middle portion of the specimens. In specimen 3, at 1.33% drift, twisting near the loading stub

beam was observed and the test was terminated due to experimental dysfunctionality. In case of specimen SW4 the test was terminated at 2% drift, when widening of the shear cracks was observed. Prior to the termination of the test, the specimens with a higher strengthening ratio observed significantly better behavior by delaying the formation of shear cracks and their propagation with the increase in drift levels. Further, most of the cracks were accumulated in the web region below the lower middle portion, attributing to the significant influence of steel wire mesh and polymer mortar. There was no debonding between polymer mortar layers and concrete surface in specimens SW3 and SW4 before the termination of the test.

In specimen SW5 ($\rho_{swm} = 0.3\%$) with the wrapping of steel wire mesh only on exposed surfaces using four anchor systems, the flexure-shear cracks were found to be lesser than that of specimen SW4 ($\rho_{swm} = 0.3\%$). Minor hairline flexural cracks initiated at 0.2% (192 kN) drift and with the increase in monitored drift, flexural cracks propagated towards the wall web at 0.66% (379 kN). In the subsequent drift levels, flexural cracks were connected with diagonal shear cracks and proliferated towards the loading and bottom corners of the specimen. After 2% (548 kN) drift level, debonding of polymer mortar layer along the height and crushing near the corners of walls was observed. The width of the cracks formed were found to be lesser than that of specimen SW3 ($\rho_{swm} = 0.2\%$). From the comparison of crack patterns and failure mechanisms of specimens SW4 and SW5, it was comprehended that application of wrapping of steel wire mesh around the surface of the specimens was found to be beneficial compared to wrapping only on exposed surfaces as it confined the specimen and avoided debonding of mortar layers and crushing of core concrete of the shear wall.

4. Experimental Results and Discussion

The application of steel wire mesh and polymer mortar to improve the behavior of seismic deficient shear walls was evaluated in terms of hysteretic and envelop lateral load-drift response, energy dissipation capacity, and analysis of strain gauge recordings in the following sections.

4.1. Hysteretic and Envelop Lateral Load-Drift Response

The hysteretic response of control and strengthened shear wall specimens is shown in Figure 7. The specimens were found to be in elastic state and no residual deformation was recorded after the completion of initial force-controlled loading. With an increase in drift levels, the web region of the shear walls observed cracking. The specimens proliferated into the elasto-plastic stage, and the residual displacement of the specimens increased significantly after unloading.

The control specimen (SW1) exhibited severe pinching at 1% (322 kN) drift, which was mainly due to the opening and closing of diagonal shear cracks. The shear cracks in the strengthened specimens (SW2 to SW5) were effectively controlled, and the hysteretic loops were plumper compared to that of control specimen SW1. Among the strengthened specimens with wrapping around the surface, the hysteretic response of SW4 specimen with a higher steel wire mesh ratio ($\rho_{swm} = 0.3\%$) observed better behavior compared to SW2 ($\rho_{swm} = 0.2\%$), and SW3 ($\rho_{swm} = 0.2\%$). The hysteretic behavior of specimens with wrapping around the surface (SW4) and only on the exposed surface (SW5) was found to be similar, except for debonding failure along the corners, which was observed in case of SW5 at 2% drift.
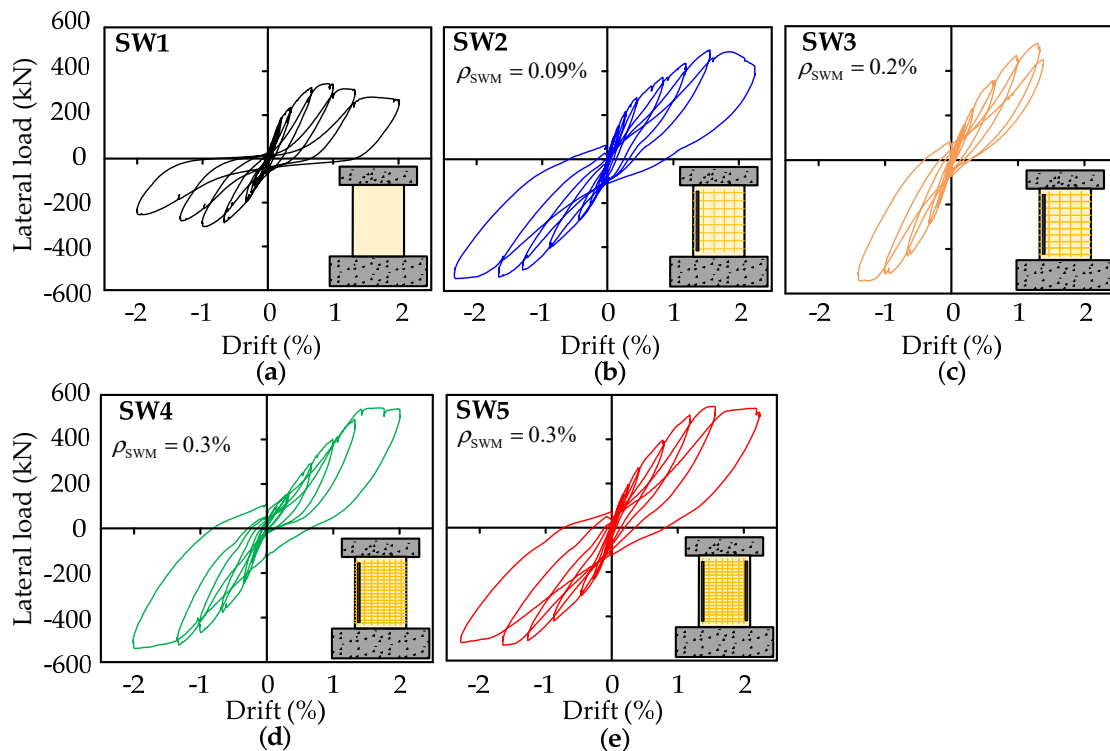
Figure 7. Hysteretic lateral load-drift response of specimens: (**a**) SW1; (**b**) SW2; (**c**) SW3; (**d**) SW4; (**e**) SW5.

The envelop and the characteristic points of the lateral load-drift response of shear wall specimens is shown in Figure 8a and Table 3, respectively. The cracking load (P_{cr}) was calculated based on the drift corresponding to the major crack formation in specimens, and yield load was determined following the equivalent energy method. It was observed that the average increase in the cracking load (P_{cr}), yield load (P_y), and the maximum capacity (P_m) of strengthened specimens was about 99%, 57%, and 54% compared to that of the control specimen, respectively. It was comprehended that all the considered characteristic loads (cracking, yielding, and maximum) increased with an increase in the steel wire reinforcement ratio (ρ_{swm}). Specimen SW4 (ρ_{swm} = 0.3%) observed a higher cracking load (7–35%) and a yielding load (6–26%) compared to other specimens SW3 and SW2. However, the increase in the peak load capacity of the specimen SW4 was found to be marginal (3–9%) compared to that of SW3 and SW2 specimens. Further, it was also observed that a decrease in diameter and spacing of steel wire mesh influenced the lateral load-drift response of specimens. The lateral load corresponding to each drift level in case of specimens SW3 and SW4 was found to be higher than that SW2, which may be due to the smaller spacing adopted, effectively restraining the web concrete from damage and improving the lateral load behavior.

Table 3. Summary of experimental results.

Specimen	P_{cr} (kN)	δ_{cr} (%)	P_y (kN)	δ_y (%)	P_m (kN)	δ_m (%)	K_i (kN/mm)	ED (kNmm)
SW1	96	0.10	285	0.52	342	0.90	92	47,600
SW2	158	0.17	383	0.98	496	1.30	106	57,700
SW3	198	0.25	456	0.94	523	1.43	109	60,200
SW4	212	0.28	485	1.31	541	1.97	105	125,800
SW5	207	0.29	468	1.03	548	1.55	95	108,600

Note: P_{cr}, P_y and P_{peak} are the cracking, yield, and peak load of the specimens, respectively, and δ_{cr}, δ_y, and δ_m represent the corresponding displacements; K_i is the initial stiffness; and *ED* is the cumulative energy dissipation.
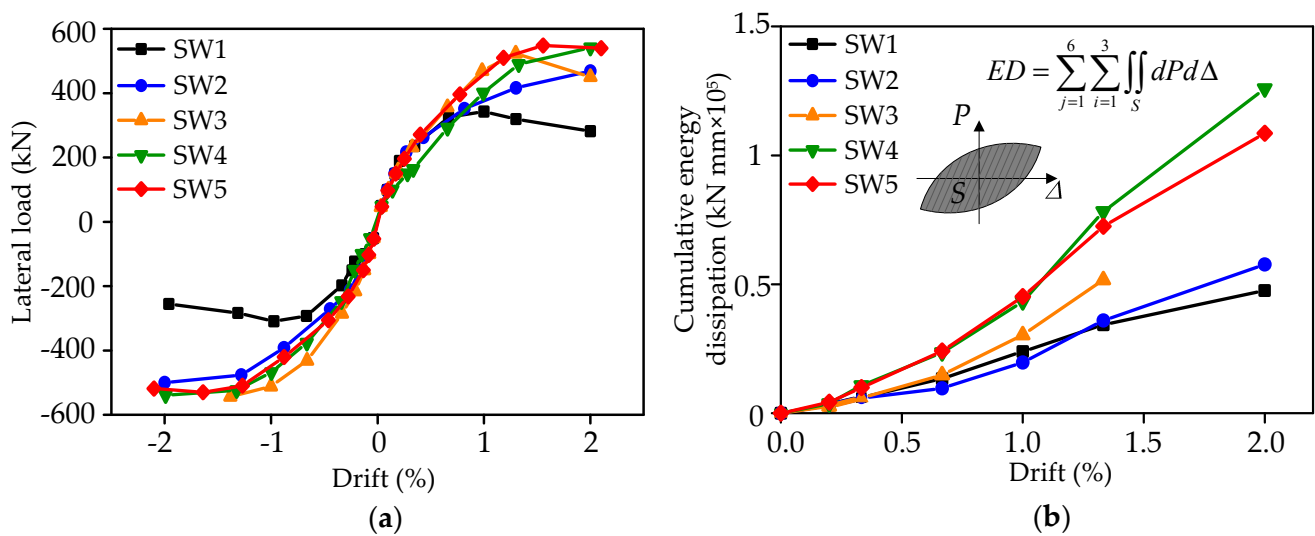
Figure 8. Comparison of: (**a**) lateral load-drift response; (**b**) cumulative energy dissipation at different drift levels.

The characteristic load points of the specimen wrapping around the surface (SW4) and only on the exposed surface (SW5) were found to be almost same. This indicated the insignificant influence of wrapping the steel wire mesh on the lateral load behavior for the considered drift levels. In the present study, initial stiffness was calculated as the secant slope connecting 5% to 33% of lateral load corresponding to the first hysteretic loop [32]. The initial stiffness of the strengthened specimens was found to be 1.03 to 1.18 times that of the control specimen (SW1). Specimen SW5 observed slightly lower initial stiffness (95 kN/mm) compared to SW4. The higher anchor bolt systems (four) and a greater number of bolt holes on the wall surface in specimen SW5 decreased the initial stiffness compared to specimens SW2–SW4. Overall, it was found that stiffness of specimens was found to be nearly identical (95 kN/mm–109 kN/mm), which indicated that the initial stiffness was not influenced by polymer mortar, steel wire ratio, and its wrapping method adopted.

4.2. Energy Dissipation

The variation of energy dissipation for different drift levels is shown in Figure 8b and the cumulative energy dissipation, calculated as the summation of the areas under the three hysteretic loops for each drift level (0.2%, 0.33%, 0.67%, 1%, 1.33%, and 2%), is given in Table 3. The energy dissipation capacity of the strengthened specimens increased significantly, and it was about 1.2 to 2 times that of the control specimen, which may be due to the confinement provided by the steel wire mesh and polymer mortar during the test. Specimen SW4 with a higher reinforcement ratio and wrapping around the surface observed higher energy dissipation capacity and it was about 2.1 times that of the control specimen SW1. The cumulative energy dissipation capacity of specimens SW2 and SW3 was found to be almost the same and it was about 1.2 times that of the control specimen. Specimen SW4 observed higher energy dissipation, which was mainly due to the smaller spacing (40 mm) of steel wire mesh adopted, which enhanced the compressive behavior of web concrete as discussed previously. The energy dissipation capacity of specimen SW5 was found to be similar as that of the SW4 specimen till 1% drift level. In the subsequent drift levels, debonding of polymer mortar layers around the edges reduced the energy dissipation capacity of specimen SW5. The cumulative energy dissipation capacity of SW5 was about 0.86 times that of the specimen SW4. From the calculation of energy dissipation capacity, it was ascertained that the wrapping of steel wires around the specimen surface with a higher percentage reinforcement ratio was found to be more effective compared to strengthening only on the exposed surfaces.

4.3. Analysis of Strain Gauge Recordings

The variation of strain recorded in the web region of specimens SW1 to SW5 corresponding to maximum load is shown in Table 4. It was observed that most of the stain gauges were found to be in tension during the entire test (Figure 9). This is mainly because of the principal tensile strain direction in the wall web being approximately consistent with the diagonal direction of the shear wall, and the principal strain developed two components of tensile strain in both horizontal and vertical directions. The horizontal strain in the wall web of control specimen SW1 observed a higher strain (2150 με–3870 με) and the utilization coefficient ranged from 0.97 to 1.75. This was further confirmed from the severe diagonal cracking observed in the wall web in control specimen SW1 (Figure 6). In case of SW2, the horizontal strain gauge (H3) at the web reached 2883 με with a utilization coefficient of 1.30. Conversely, the horizontal reinforcement in the web of specimens SW3 and SW4 recorded slightly lesser strain [2462 με (1.11), and 2097 με (0.95)]. It was found that strain in the reinforcement near the middle of the web region decreased with increase in reinforcement ratio ρ_{swm}. In specimen SW5, the horizontal strain gauge (H3) observed higher strain (3664 με, 1.66) compared to SW4 (2097 με, 0.95), which may be due to the wrapping methods adopted. The peak values of vertical strain gauges in the wall web region decreased with as increase in steel wire ratio (ρ_{swm}), as shown in Figure 9b.

Table 4. Strain gauge recordings corresponding to peak load.

Specimen	Strain (με)									
	H1	**V1**	**H2**	**V2**	**H3**	**V3**	**H4**	**V4**	**H5**	**V5**
SW1	2529 (1.14) *	607 (0.27)	2269 (1.03)	1197 (0.54)	2804 (1.27)	2359 (1.07)	3550 (1.61)	2150 (0.97)	3870 (1.75)	1742 (0.79)
SW2	2207 (1.00)	1187 (0.54)	1678 (0.76)	1024 (0.46)	2883 (1.30)	1641 (0.74)	3061 (1.39)	1884 (0.85)	3390 (1.53)	1910 (0.86)
SW3	1316 (0.60)	863 (0.39)	1774 (0.80)	1099 (0.50)	2462 (1.11)	1448 (0.66)	2743 (1.24)	1832 (0.83)	3080 (1.39)	1448 (0.66)
SW4	1764 (0.80)	589 (0.27)	2141 (0.97)	826 (0.37)	2097 (0.95)	1360 (0.62)	2303 (1.04)	1417 (0.64)	2364 (1.07)	1525 (0.69)
SW5	1784 (0.81)	433 (0.20)	2059 (0.93)	770 (0.35)	3664 (1.66)	1529 (0.69)	2406 (1.09)	1585 (0.72)	2584 (1.17)	1473 (0.67)

Note: * Figures in the brackets represent utilization coefficient of steel (α) calculated as the ratio of strain recorded to the yield strain of the steel reinforcement.
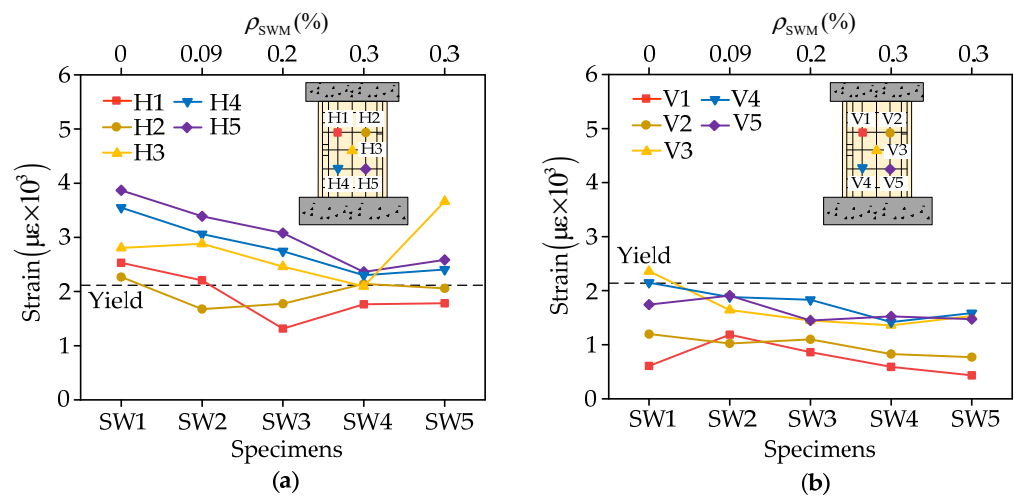

Figure 9. Variation of strain corresponding to peak load at various locations in: (**a**) horizontal and (**b**) vertical directions.

Overall, it was observed that most of strain gauge recordings in the web region were in tension during the test and the smaller values of strain recorded in specimen SW4 because

of its higher strengthening ratio of SWM (0.3%), compared to other specimens SW2 (0.09%) and SW3 (0.2%). Furthermore, the strain values varied with observed failure modes of the specimens. Specimens SW1–SW2 observed diagonal shear cracks predominantly and higher tensile strain in the horizontal reinforcement. On the other hand, specimens SW3, SW4, and SW5 observed flexure-shear cracks in which the horizontal reinforcement was subjected to lower tensile strain. It was comprehended that specimens with high steel wire mesh ratio exhibited better effectiveness in restricting the crack propagation and the failure mode was modified from brittle shear failure to ductile flexure-shear failure.

5. Estimation of Shear Capacity of Strengthened Shear Walls

In the present study, theoretical analysis was carried out to predict the shear strength of strengthened shear walls. The effective coefficient of the steel wire mesh was derived based on the softened strut-and-tie model [33]. The expression recommended in ACI 318 [1] was modified to predict the capacity of the shear walls considering the influence of steel wire mesh reinforcement ratio and polymer mortar. The nominal shear capacity (V_n) of the conventional shear wall estimated following ACI 318, and is calculated as the summation of the contribution of concrete and distributed transverse reinforcement, given in Equation (1).

$$V_n = \alpha_c \lambda \sqrt{f_c'} A_{cv} + f_y A_s \tag{1}$$

where α_c is the coefficient to define the relative contribution of concrete strength to nominal wall shear strength, which linearly varied between 3 and 2 for 1.5 < H/L < 2.0; λ is the modification factor to consider the reduced mechanical properties of lightweight concrete relative to normal weight concrete; f_c' is the compressive strength of concrete; f_y is the yield strength of reinforcement; A_{cv} and A_s are the gross area of concrete section and the transverse reinforcement, respectively. The capacity of the strengthened shear wall (V_{ns}) considering the contribution of steel wire mesh and polymer mortar is given in Equation (2).

$$V_{ns} = \alpha_c \lambda \sqrt{f_c'} \left(A_{cv} + \frac{E_m}{E_c} A_m \right) + f_y A_s + \beta f_{yw} A_{hw} \tag{2}$$

where E_m and E_c are the elasticity modulus of polymer and concrete, respectively (Table 2); A_m is the area of polymer mortar layers; β is the effective coefficient of the steel wire mesh; f_{yw} is the ultimate tensile strength of steel wire; A_{hw} is the area of the horizontal SWM layers. In the present study, the effective coefficient (β) was derived following the softened strut-and-tie model (STM). To finalize the resistance model following the principles of equilibrium, the differential expression of shear force can be written as

$$V = \frac{dM}{dx} = \frac{d(T \cdot L)}{dx} = \frac{dT}{dx}L + \frac{dL}{dx}T \tag{3}$$

where M and V represent the bending moment and shear force, respectively; T is the tensile force of longitudinal reinforcement; L is the internal moment arm (Figure 10). The two terms on the right-hand side of Equation (3) represent the arch (Figure 10a) and truss (Figure 10b) mechanisms by which the external shear force was resisted. Further, the combined force analysis of arch and truss mechanisms is shown in Figure 10c.

The arch mechanism (V_{h1}) was taken as diagonal compression force in the strut ($D \cos \theta$), whereas the truss mechanism (V_{h2}) includes horizontal ties and two struts. During the tests, most of the horizontal strain gauges in the wall web exceeded yielding (2210 $\mu\varepsilon$), as shown in Figure 9a, as soon as the specimens attained the peak load capacity. For this reason, the resistance provided by the horizontal ties was taken as a combination of the contribution of transverse reinforcement and steel wire mesh (Equation (5)).

$$V_h = V_{h1} + V_{h2} = -D \cos \theta + F_h \tag{4}$$
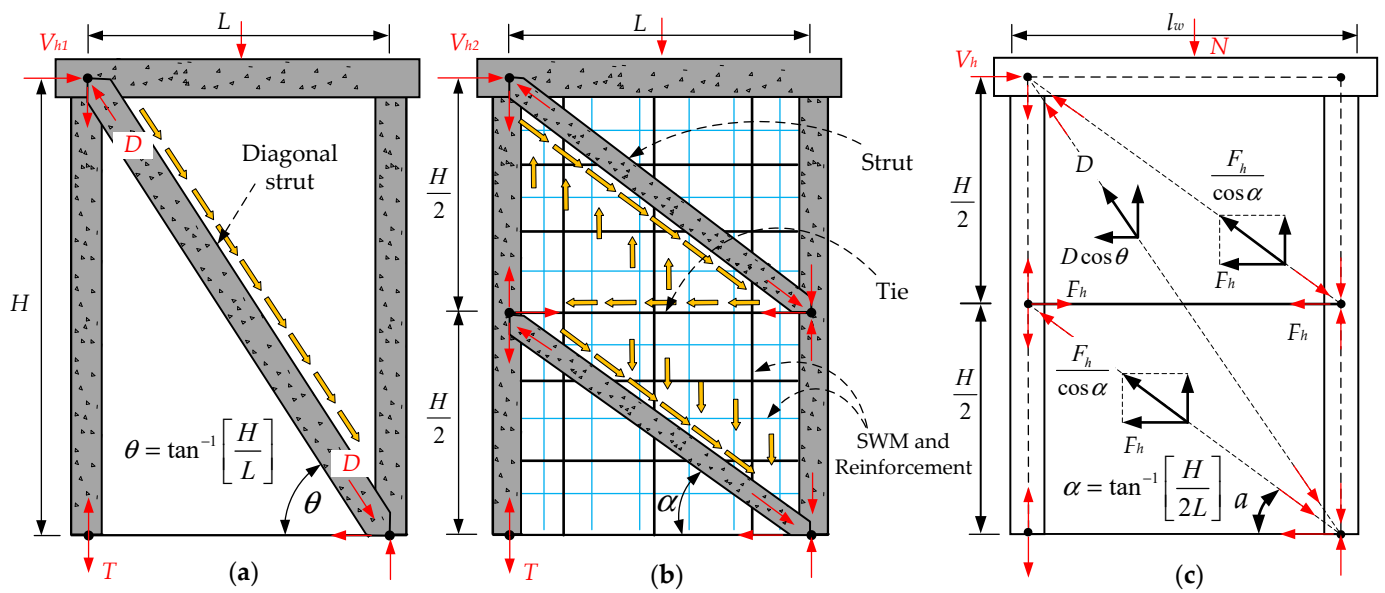
$$F_h = f_y A_{hs} + \beta f_{yw} A_{hw} \tag{5}$$

Figure 10. Shear wall resisting mechanisms: (**a**) arch mechanism; (**b**) truss mechanism; (**c**) combined force analysis of arch and truss mechanisms.

According to Jennewein and Schäfer [34], the stiffness ratio between the truss mechanism and the arch mechanism to transfer the horizontal shear is given by $\gamma_h/(1 - \gamma_h)$. γ_h represents the fraction of horizontal shear transferred by the horizontal tie (Equation (6)). Therefore, the external lateral shear force (V_h) must be apportioned to the truss and arch mechanisms as given in Equation (7).

$$\gamma_h = \frac{2\tan\theta - 1}{3}, \quad 0 \le \gamma_h \le 1 \tag{6}$$

$$F_h : -D\cos\theta = \gamma_h : (1 - \gamma_h) \tag{7}$$

Since the external lateral shear force (V_h) is mainly transferred in the major stress direction of the wall web, the average principal compressive stress σ_d is assumed to govern the failure [33]. The combined truss and arch mechanisms can be estimated considering the compressive stress field distribution and cartesian transformation (Figure 11), as shown in Equation (8).

$$V_h = -\sigma_d A_{str} \cos\varphi = -D\cos(\theta - \varphi)\cos\varphi + \frac{F_h}{\cos\alpha} \times \cos(\varphi - \alpha)\cos\varphi \tag{8}$$

where σ_d represents the average principal compressive stress of concrete (here a positive sign represents tension) resulting from compressive forces from arch and truss mechanisms; A_{str} represents the effective area of the diagonal strut; φ is the angle between the principal stress and the horizontal direction.

The angle φ was calculated as per eigenvalue calculation considering the average major horizontal (ε_h) and vertical tensile (ε_v), and diagonal compressive strains (ε_d) as shown in Figure 11. The shear strain (γ) is an unknown parameter and is determined following the principles of similar matrices in Linear algebra (determinants of the similar matrices are equal). It is assumed that eigenvalue vector x can be written as $x = (a, b)^T$. The eigenvalue vector x corresponding to strain matrix A is the direction vector of principal strain direction. Using the trigonometric relationships, the angle φ between the principal stress and the horizontal direction can be obtained. Hwang and Lee [35] reported that the average principal compressive strain (ε_d) was linearly varied from -0.001 to 0 for shear walls with shear span ratios of 1 to 3, respectively. The average principal compressive strain ε_d in the present study was about $-690\,\mu\varepsilon$ as the shear span ratio of specimens was

1.62. The average principal tensile strain ε_r was calculated as per the first strain invariant as follows.

$$\varepsilon_r = \varepsilon_h + \varepsilon_v - \varepsilon_d \tag{9}$$

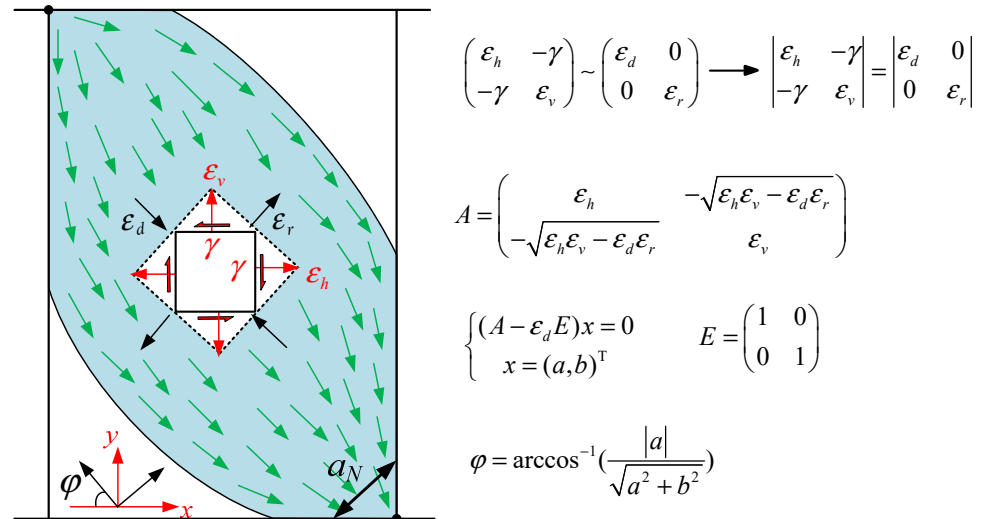$$\begin{pmatrix} \varepsilon_h & -\gamma \\ -\gamma & \varepsilon_v \end{pmatrix} \sim \begin{pmatrix} \varepsilon_d & 0 \\ 0 & \varepsilon_r \end{pmatrix} \longrightarrow \begin{vmatrix} \varepsilon_h & -\gamma \\ -\gamma & \varepsilon_v \end{vmatrix} = \begin{vmatrix} \varepsilon_d & 0 \\ 0 & \varepsilon_r \end{vmatrix}$$

$$A = \begin{pmatrix} \varepsilon_h & -\sqrt{\varepsilon_h \varepsilon_v - \varepsilon_d \varepsilon_r} \\ -\sqrt{\varepsilon_h \varepsilon_v - \varepsilon_d \varepsilon_r} & \varepsilon_v \end{pmatrix}$$

$$\begin{cases} (A - \varepsilon_d E)x = 0 \\ x = (a,b)^{\mathrm{T}} \end{cases} \qquad E = \begin{pmatrix} 1 & 0 \\ 0 & 1 \end{pmatrix}$$

$$\varphi = \arccos^{-1}\left(\frac{|a|}{\sqrt{a^2+b^2}}\right)$$

Figure 11. Compression stress field.

The average horizontal tensile strain ε_h and the average vertical tensile strain ε_v were taken as +0.002 and +0.001 based on the observations of strain recordings, respectively. The unknown variable of effective area of the diagonal strut A_{str} was defined in Equation (10).

$$A_{str} = a_N \times t_w \tag{10}$$

where a_N is the equivalent width of the principal stress strut (Figure 11) and can be approximated using Paulay and Priestley's [36] equation for the depth of the flexural compression zone of an elastic column as follows.

$$a_N = \left(0.25 + 0.85\frac{N}{A_w f'_c}\right) l_w \tag{11}$$

where A_w is the net area of the concrete section bounded by the web thickness (t_w) and the length of the section in the direction of the shear force (l_w). It has to be noted that in the strut-and-tie model, the axial compression not only delayed the softening effect of concrete but also increased the cross-sectional area of the principal strut. The average principal compressive stress of concrete (σ_d) was calculated based on the ascending branch of the softened stress-strain curve of the cracked concrete model proposed by Zhang and Hsu [37] and is given in Equation (12).

$$\sigma_d = -\zeta f'_c\left[2\left(\frac{-\varepsilon_d}{\zeta\varepsilon_0}\right) - \left(\frac{-\varepsilon_d}{\zeta\varepsilon_0}\right)^2\right], \quad \text{for} \quad \frac{-\varepsilon_d}{\zeta\varepsilon_0} \leq 1 \tag{12}$$

$$\zeta = \frac{5.8}{\sqrt{f_c}}\frac{1}{\sqrt{1+400\varepsilon_r}} \leq \frac{0.9}{\sqrt{1+400\varepsilon_r}} \tag{13}$$

where ζ is the softening coefficient and ε_0 is the strain corresponding to the concrete cylindrical strength f'_c which can be estimated using the Equation (14) proposed by Foster and Gilbert [38].

$$\varepsilon_0 = 0.002 + 0.001\left(\frac{f'_c - 20}{80}\right) \quad \text{for} \quad 20 \leq f'_c \leq 100 \text{ MPa} \tag{14}$$

The effectiveness coefficient (β) of steel wire mesh is calculated using Equation (15), by solving Equations (4)–(14). The flowchart of the solution procedure to estimate the effectiveness coefficient (β) is shown in Figure 12.

$$\beta = \left(\frac{-\sigma_d A_{str} \gamma_h \cos\varphi \cos\theta \cos\alpha}{[(1-\gamma_h)\cos(\theta-\varphi)\cos\varphi\cos\alpha + \gamma_h \cos(\varphi-\alpha)\cos\varphi\cos\theta] f_{yw} A_{hw}} \right) - \frac{f_y A_{hs}}{f_{yw} A_{hw}} \tag{15}$$
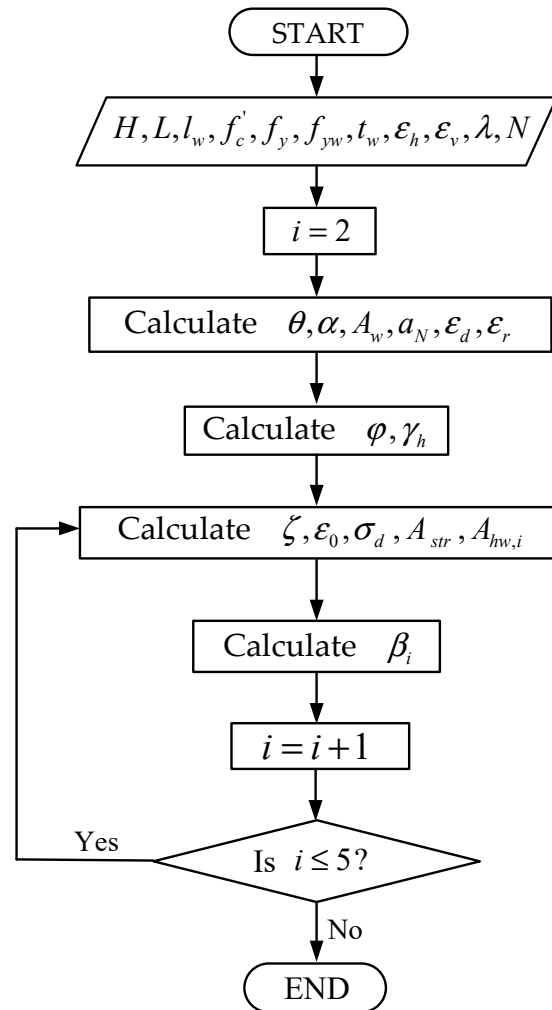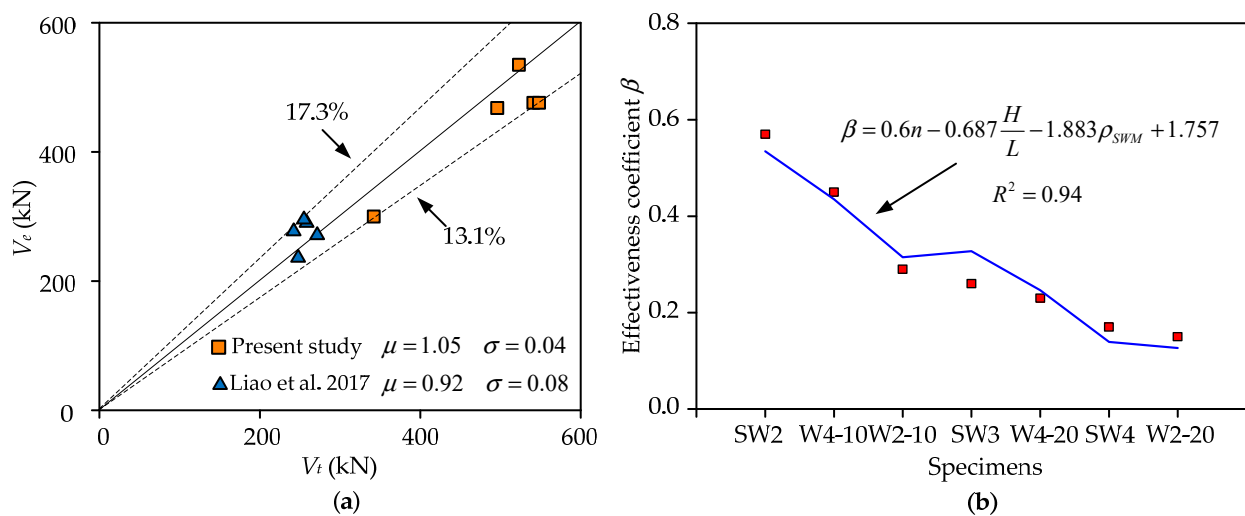

Figure 12. Flowchart to estimate the effectiveness coefficient of steel wire mesh β.

Table 5 shows the comparison of the shear capacity of RC shear walls between the experimental (V_e) and predicted (V_t) results. It was observed that the influence of effectiveness coefficient (β) decreased with an increase in steel wire mesh strengthening ratio. The effect of strengthening options wrapping around or only on exposed surfaces to estimate β was not considered as the shear capacity of specimens (SW4 and SW5) was found to be very close. The mean value (μ) and standard deviation (σ) of V_e/V_t was found to be about 1.05 and 0.04, respectively. This clearly showed that the proposed expression accurately predicted the shear capacity of the shear wall strengthened with SWM.

Table 5. Comparison between experimental results and theoretical values.

Reference Study	Specimen	n	H/L	ρ_{swm} (%)	β	V_e (kN)	V_t (kN)	V_e/V_t
Present Study	SW1	0.1	1.62	-	-	342	319	1.07
	SW2	0.1	1.62	0.09	0.57	496	468	1.02
	SW3	0.1	1.62	0.20	0.26	523	535	0.98
	SW4	0.1	1.62	0.30	0.17	541	476	1.08
	SW5	0.1	1.62	0.30	0.17	548	476	1.10
Liao et al. [39]	W2-10	0.2	2.00	0.10	0.29	242	280	0.86
	W2-20	0.2	2.00	0.20	0.15	271	274	0.99
	W4-10	0.4	2.00	0.10	0.45	254	298	0.85
	W4-20	0.4	2.00	0.20	0.23	258	293	0.88

In order to verify the suitability of the proposed expression, a comparative study was carried out to estimate the shear capacity of specimens tested in the previous study by Liao et al. [39], and is given in Table 5 and Figure 13. The proposed expression reasonably estimated the shear capacity of the strengthened specimens as in the case of Liao et al. [39], and the ratio was in the range of 0.85–0.99. The mean and the standard deviation of V_e/V_t were found to be about 0.92 and 0.08, respectively. Considering the maximum upper bound (17.3%) and lower bound (13.1%) deviations (Figure 13), it was apprehended that the lateral load capacity of RC shear walls strengthened with steel wire meshes can be predicted fairly using the proposed expression.

Figure 13. (**a**) Comparison of experimental and theoretical shear strength results; (**b**) multiple linear regression analysis fitted curve of effectiveness coefficient (β).

The proposed expression Equation (15) to estimate the effectiveness coefficient is slightly complex in nature to be used in practical engineering purposes. Henceforth, multiple linear regression analysis was carried out and a simplified empirical expression (Equation (16)) was proposed to predict β as a function of n, H/L, and ρ_{swm}. The effectiveness coefficient β is significantly influenced by the strengthening ratio (1.883) compared to the axial compression n (0.6) and shear span ratio H/L (0.687). The multiple linear regression expression with a favorable coefficient of determination ($R^2 = 0.94$) is presented in Figure 13b, from which it can be ascertained that β generally tends to decrease with an increase in H/L and ρ_{swm}. Conversely, β was found to increase with an increase in n, and this is likely due to the axial compression force, which increased the width of the strut in the strut-and-tie-model. Due to the limitation in the number of experimental investigations,

further research needs to be conducted to provide a more reliable expression to estimate the effectiveness coefficient of the steel wire mesh.

$$\beta = 0.6n - 0.687\frac{H}{L} - 1.883\rho_{\text{SWM}} + 1.757 \quad \left\{ \begin{array}{c} 0.1 \leq n \leq 0.4 \\ 0.09\% \leq \rho_{\text{SWM}} \leq 0.3\% \\ 1.62 \leq H/L \leq 2 \end{array} \right. \tag{16}$$

6. Conclusions

Lateral load behavior of existing shear walls strengthened with steel wire meshes and polymer mortar were investigated in the present study. Four strengthened specimens and one control specimen considering different steel wire mesh reinforcement ratios and wrapping methods were tested under cyclic lateral loading. Further, a detailed theoretical analysis was carried out to predict the shear capacity of the strengthened shear wall specimens. The main conclusions drawn from this research are as follows:

- Steel wire mesh and polymer mortar strengthening method not only delayed the formation of shear cracks but also effectively restrained the crack propagation, which significantly increased the cracking load (average increase was about 79%). The capacity of the strengthened shear wall specimens increased with an increase in the reinforcement ratio of steel wire mesh. The average increase in capacity was found to be 55%, showing a favorable strengthening effect;
- The hysteretic response of strengthened specimens was found to be plumper compared to control RC specimen, which exhibited severe pinching. Wrapping of steel wire meshes around the specimen surface avoided the debonding failure of polymer mortar layers and enhanced the energy dissipation characteristics compared to wrapping only on exposed surfaces;
- The effectiveness coefficient to consider the contribution of steel wire mesh was derived to predict the capacity of strengthened shear wall specimens based on the softened strut-and-tie model. The proposed expression can be used to fairly predict the shear capacity of the strengthened specimens (present and previous experimental studies) within the scope of variables (n = 0.1–0.4, H/L = 1.62–2, and ρ_{swm} = 0.09–0.3%);
- Further from the limited theoretical investigation, it was also ascertained that the effectiveness coefficient of steel wire mesh was affected by the steel wire ratio, shear span ratio, and axial compression ratio. A steel wire mesh reinforcement ratio of about 0.1–0.2% was recommended to adopt in the strengthening of existing RC shear walls within the scope of the shear span ratio (1.62 to 2.00).

References

1. *ACI Committee 318*; Building Code Requirements for Structural Concrete and Commentary (ACI CODE 318-19). American Concrete Institute: Indianapolis, IN, USA, 2019.
2. *EN 1998-1-1*; Eurocode 8: Design of Structure for Earthquake Resistance-Part 1: General Rules, Seismic Actions and Rules for Building. CEN: Brussels, Belgium, 2004.
3. CMC (China Ministry of Construction). *GB 50011-2010*; Code for Seismic Design of Buildings. China Architecture & Building Press: Beijing, China, 2011. (In Chinese)
4. Xu, P.; Huang, J.; Chen, F. Earthquake damages to shear wall structure in last fifty years and seismic design enlightenment. *J. Build. Struct.* **2017**, *38*, 1–13. (In Chinese)
5. Wallace, J. Performance of structural walls in recent earthquakes and test and implications for US building codes. In Proceedings of the 15th World Conference on Earthquake Engineering, Lisbon, Portugal, 24–28 September 2012.
6. Kam, W.Y.; PaMPanin, S.; Elwood, K.J. Seismic performance of reinforced concrete buildings in the 22 February Christchurch (Lyttleton) earthquake. *Bull. N. Z. Nat. Soc. Earthq. Eng.* **2011**, *44*, 239–278.
7. Woods, J.E.; Lau, D.T.; Cruz-Noguez, C.A. In-Plane seismic strengthening of nonductile reinforced concrete shear walls using externally bonded CFRP sheets. *J. Compos. Constr.* **2016**, *20*, 04016052. [CrossRef]
8. Marini, A.; Meda, A. Retrofitting of RC shear walls by means of high-performance jackets. *Eng. Struct.* **2009**, *31*, 3059–3064. [CrossRef]
9. Altin, S.; Kopraman, Y.; Baran, M. Strengthening of RC walls using externally bonding of steel strips. *Eng. Struct.* **2013**, *49*, 686–695. [CrossRef]
10. Christidis, K.I.; Vougioukas, E.; Trezos, K.G. Strengthening of non-conforming RC shear walls using different steel configurations. *Eng. Struct.* **2016**, *124*, 258–268. [CrossRef]
11. Antoniades, K.K.; Salonikios, T.N.; Kappos, A.J. Tests on seismically damaged reinforced concrete walls repaired and strengthened using Fiber-Reinforced Polymers. *J. Compos. Constr.* **2005**, *9*, 236–246. [CrossRef]
12. Li, B.; Lim, C.L. Tests on seismically using Fiber-reinforced Polymers. *J. Compos. Constr.* **2010**, *14*, 597–608. [CrossRef]
13. Layssi, H.; Cook, W.D.; Mitchell, D. Seismic response and CFRP retrofit of poorly detailed shear walls. *J. Compos. Constr.* **2012**, *17*, 603–613. [CrossRef]
14. EI-Sokkary, H.; Galal, K. Seismic Behavior of RC shear walls strengthened with Fiber-Reinforced Polymer. *J. Compos. Constr.* **2013**, *17*, 603–613. [CrossRef]
15. EI-Sokkary, H.; Galal, K.; Ghorbanirenani, I.; Léger, P.; Tremblay, R. Shake table test on FRP-Rehabilitated RC shear walls. *J. Compos. Constr.* **2013**, *17*, 79–90. [CrossRef]
16. Qazi, S.; Michel, L.; Ferrier, E. Seismic behaviour of RC short shear wall strengthened with externally bonded CFRP strips. *Compos. Struct.* **2019**, *211*, 390–400. [CrossRef]
17. Fontanari, V.; Benedetti, M.; Monelli, B.D.; Degasperi, F. Fire behavior of steel wire ropes: Experimental investigation and numerical analysis. *Eng. Struct.* **2015**, *84*, 340–349. [CrossRef]
18. Al-Kaimakchi, A.; Rambo-Roddenberry, M. Measured transfer length of 15.2-mm (0.6-in.) duplex high-strength stainless steel strands in pretensioned girders. *Eng. Struct.* **2021**, *237*, 112178. [CrossRef]
19. Kumar, V.; Patel, P.V. Strengthening of axially loaded circular concrete columns using stainless SWM (SSWM)–Experimental investigations. *Constr. Build. Mater.* **2016**, *12*, 4186–4198.
20. Kim, S.Y.; Yang, K.H.; Byun, H.Y.; Ashour, A.F. Tests of reinforced concrete beams strengthened with wire rope units. *Eng. Struct.* **2007**, *29*, 2711–2722. [CrossRef]
21. Yang, K.; Byun, H.; Ashour, A.F. Shear strengthening of continuous reinforced concrete T-beams using wire rope units. *Eng. Struct.* **2009**, *31*, 1154–1165. [CrossRef]
22. Banerjee, S.; Nayak, S.; Das, S. Shear and flexural behaviour of unreinforced masonry wallets with SWM. *J. Build. Eng.* **2020**, *30*, 101254. [CrossRef]
23. Sandoval, O.J.; Takeuchi, C.; Carrillo, J.; Barahona, B. Performance of unreinforced masonry panels strengthened with mortar overlays reinforced with welded wire mesh and horizontal connectors. *Constr. Build. Mater.* **2021**, *267*, 121054. [CrossRef]
24. Yao, X.; Guo, Z.; Basha, S.H.; Huang, Q. Innovative seismic strengthening of historic masonry walls using polymer mortar and steel strips. *Eng. Struct.* **2021**, *228*, 111507. [CrossRef]
25. Zhang, X.; Du, M.; Fang, H.; Shi, M.; Zhang, C.; Wang, F. Polymer-modified cement mortars: Their enhanced properties, applications, prospects, and challenges. *Constr. Build. Mater.* **2021**, *299*, 124290. [CrossRef]
26. Shermi, C.; Dubey, R.N. Study on out-of-plane behaviour of unreinforced masonry strengthened with welded wire mesh and mortar. *Constr. Build. Mater.* **2017**, *143*, 104–120. [CrossRef]
27. Shermi, C.; Dubey, R.N. In-plane behaviour of unreinforced masonry panel strengthened with welded wire mesh and mortar. *Constr. Build. Mater.* **2018**, *178*, 195–203. [CrossRef]
28. CMC (China Ministry of Construction). *JGJ 3-1991*; Standard for Structural Design and Construction of Reinforced Concrete High-Rise Buildings. China Architecture & Building Press: Beijing, China, 1991. (In Chinese)
29. CMC (China Ministry of Construction). *GB/T 50081-2002*; Standard for Test Method of Mechanical Properties on Ordinary Concrete. China Architecture & Building Press: Beijing, China, 2002. (In Chinese)

30. CMC (China Ministry of Construction). *JGJ/T70-2009*; Standard for Test Method of Performance on Building Mortar. China Architecture & Building Press: Beijing, China, 2009. (In Chinese)
31. CMC (China Ministry of Construction). *JGJ 101-1996*; Specificating of Testing Methods for Earthquake Resistant Building. China Architecture & Building Press: Beijing, China, 1996. (In Chinese)
32. Basha, S.H.; Kaushik, H.B. Behavior and failure mechanisms of masonry-infilled RC frames (in low-rise buildings) subject to lateral loading. *Eng. Struct.* **2016**, *111*, 233–245. [CrossRef]
33. Hwang, S.; Fang, W.; Lee, H.; Yu, H. Analytical model for predicting shear strengthof squat walls. *J. Struct. Eng.* **2001**, *127*, 43–50. [CrossRef]
34. Jennewein, M.; Schafër, K. *DafStb Heft 430*; Standardisierte Nachweise Vonhaufigen D-Bereichen. Beuth: Berlin, Germany, 1992.
35. Hwang, S.; Lee, H. Strength Prediction for discontinuity regions by softened strut-and-tie model. *J. Struct. Eng.* **2002**, *128*, 1519–1526. [CrossRef]
36. Paulay, T.; Priestley, M.J.N. *Seismic Design of Reinforced Concrete and Masonry Buildings*; Wiley: New York, NY, USA, 1992.
37. Zhang, L.X.B.; Hsu, T.T.C. Behavior and analysis of 100 MPa concrete membrane elements. *J. Struct. Eng.* **1998**, *124*, 24–34. [CrossRef]
38. Foster, S.J.; Gilbert, R.I. The design of nonflexural members with normal and high-strength concrete. *ACI Struct. J.* **1996**, *93*, 3–10.
39. Liao, W.; Zhang, C.; Jia, T.; Wang, H. Experimental investigation on seismic behavior of shear wall retrofitted with pre-stressed steel wire mesh and polymer mortar. *J. Build. Struct.* **2017**, *38*, 70–77. (In Chinese)